https://doi.org/10.1093/plphys/kiac058 PLANT PHYSIOLOGY 2022: 189: 112–128

Plant Physiology®

Research Article

True oxygen reduction capacity during photosynthetic electron transfer in thylakoids and intact leaves

Duncan Fitzpatrick [1], **Eva-Mari Aro** [1,†] **and Arjun Tiwari** [1,*]

1 Department of Life Technologies, Molecular Plant Biology Unit, University of Turku, FI-20014 Turku, Finland

*Author for correspondence: arjun.tiwari@utu.fi

†Senior author

A.T., D.F., and E.-M.A. designed the research. A.T. and D.F. performed the research. A.T., D.F., and E.-M.A. analyzed the data. D.F., A.T., and E.-M.A. wrote the article.

The authors responsible for distribution of materials integral to the findings presented in this article in accordance with the policy described in the Instructions for Authors (https://academic.oup.com/plphys/pages/general-instructions) are: Eva-Mari Aro (evaaro@utu.fi) and Arjun Tiwari (arjun.tiwari@utu.fi).

Abstract

Reactive oxygen species (ROS) are generated in electron transport processes of living organisms in oxygenic environments. Chloroplasts are plant bioenergetics hubs where imbalances between photosynthetic inputs and outputs drive ROS generation upon changing environmental conditions. Plants have harnessed various site-specific thylakoid membrane ROS products into environmental sensory signals. Our current understanding of ROS production in thylakoids suggests that oxygen (O_2) reduction takes place at numerous components of the photosynthetic electron transfer chain (PETC). To refine models of site-specific O_2 reduction capacity of various PETC components in isolated thylakoids of *Arabidopsis thaliana*, we quantified the stoichiometry of oxygen production and consumption reactions associated with hydrogen peroxide (H_2O_2) accumulation using membrane inlet mass spectrometry and specific inhibitors. Combined with P700 spectroscopy and electron paramagnetic resonance spin trapping, we demonstrate that electron flow to photosystem I (PSI) is essential for H_2O_2 accumulation during the photosynthetic linear electron transport process. Further leaf disc measurements provided clues that H_2O_2 from PETC has a potential of increasing mitochondrial respiration and CO_2 release. Based on gas exchange analyses in control, site-specific inhibitor-, methyl viologen-, and catalase-treated thylakoids, we provide compelling evidence of no contribution of plastoquinone pool or cytochrome *b6f* to chloroplastic H_2O_2 accumulation. The putative production of H_2O_2 in any PETC location other than PSI is rapidly quenched and therefore cannot function in H_2O_2 translocation to another cellular location or in signaling.

Introduction

Plants exploit a range of redox balancing and signaling mechanisms to maintain an energetic homeostasis in chloroplasts, particularly important under fluctuating light conditions. These mechanisms alleviate over-excitation and over-reduction of critical photosynthetic electron transfer chain (PETC) components that may generate reactive oxygen species (ROS). Although ROS formation within the photosynthetic apparatus contributes to photodamage, they also function as critical feedback mechanisms and chemical

Received December 13, 2021. Accepted January 24, 2022. Advance access publication February 15, 2022

messengers to modify and restore an optimal redox balance. Because ROS formation occurs at the crossroads between photosynthetic damage and regulation, the elucidation of the specific locations and mechanisms of photosynthetically derived ROS generation is critical for understanding the interactions between photodamage and photoprotection. Such knowledge is central for future projects aimed at improving photosynthetic productivity.

Understanding site-specific ROS formation within the thylakoid membrane is complicated by the fact that the various components of the PETC participate in several redox reactions, forming a variety of site-specific ROS molecules with varying reactivity and reaction products. For example, during conditions of over-excitation, highly reactive and long-lived chlorophyll triplet states can form and photosensitize molecular oxygen (O_2) to singlet oxygen ($^1O_2$) (Halliwell and Gutteridge, 1984). This short-lived and highly reactive form of oxygen is mostly associated with photosystem II (PSII) (Durrant et al., 1990; Telfer et al., 1999) and leads to rapid peroxidation of proteins, lipids, and nucleotides. On the other hand, electron transfer within the PETC can result in the reduction of O_2 to form the superoxide anion ($O_2^{-\bullet}$). This reaction was originally described by Mehler (1951) and occurs primarily at the acceptor side of PSI (Mehler, 1951; Furbank and Badger, 1983). To counter this reaction, the catalyst superoxide dismutase (SOD) enzymatically dismutates two $O_2^{-\bullet}$ molecules into the oxidant hydrogen peroxide (H_2O_2), with a release of one O_2. Although H_2O_2 is relatively stable in biological systems, further reduction of H_2O_2 can result in the formation of highly destructive hydroxyl radicals ($HO^{\bullet}$). To minimize potential damage from such destructive molecules, strong ROS scavenging systems comprising peroxiredoxins, ascorbate, and ascorbate peroxidase enzymes (Asada, 2006) operate in both the thylakoid membrane and in the stroma. They facilitate the complete enzymatic two-electron reduction and protonation of H_2O_2, thereby yielding two water molecules and completing an electron pathway described as the water–water cycle (WWC) (Asada, 1999). Despite the antioxidant systems that can efficiently quench ROS, a growing body of evidence suggests that photosynthetically derived ROS such as H_2O_2 act in environmental sensing (Mubarakshina and Ivanov, 2010) and intercellular relay of information (Fichman et al., 2019) or function directly as a retrograde signal exported from the chloroplasts to the nucleus (Exposito-Rodriguez et al., 2017; Gollan and Aro, 2020).

Numerous strategies to measure site-specific ROS formation in PETC have been developed and applied over several decades, using isolated photosynthetic complexes, thylakoid membranes, or intact leaves. The resulting literature suggests that in addition to the Mehler reaction at PSI, $O_2^{-\bullet}$ and H_2O_2 can form within the PETC at heavily reduced PSII (Tiwari and Pospisil, 2009), the PQ pool (Khorobrykh and Ivanov, 2002; Mubarakshina and Ivanov, 2010; Mubarakshina Borisova et al., 2012; Khorobrykh et al., 2015), plastid terminal oxidase (PTOX) (Heyno et al., 2009), and cytochrome b_6f (Cyt-b_6f) complex (Baniulis et al., 2013). The current work aimed at resolving whether the $O_2^{-\bullet}$ produced in these different sites is rapidly quenched or whether it can induce an accumulation of H_2O_2 in PETC that can migrate from one cellular location to another and allows H_2O_2 to function as a secondary messenger for plant acclimation to specific environmental cues. To this end, by using strict biophysical and biochemical controls, we measured the true capacity of oxygen reduction/consumption at different sites in PETC (PSI, PSII, PQ-pool, and Cyt-*b6f*) in proportion to the PSII water oxidation rates.

It is necessary to revisit site-specific ROS formation in the thylakoid membrane, incorporating stronger controls, higher precision and with the capacity to discriminate O_2 reduction and true H_2O_2 accumulation. Incorporating lessons from our recent finding of the failure of DNP-INT to completely block electron transfer to PSI (Fitzpatrick et al., 2020), we have taken a methodical three-step approach to re-examine H_2O_2 formation and accumulation in isolated thylakoids of Arabidopsis (*Arabidopsis thaliana*) and have then tested our conclusions in vivo.

As the first step, to avoid artifacts from any residual activity of the PSI Mehler reaction, we measured P700 redox kinetics under experimental conditions to verify that each PETC inhibitor (Figure 1, as described schematically) completely blocked the re-reduction of oxidized P700 ($P700^+$). As the second step, we took advantage of the fact that isolated thylakoids lack the stroma and terminal electron acceptor $NADP^+$, and thus the electrons derived from oxidation of H_2O at PSII are transferred terminally to O_2 via the PETC. The overall process can be dissected into partial reactions (Asada, 2006; Figure 1, Reactions 1–4). These partial reactions can be estimated from the stoichiometry of O_2 produced and O_2 consumed at each step. Reaction (1)—The oxidation of two H_2O molecules at PSII releases one O_2 and four electrons into the PETC. Reaction (2)—The four electrons reduce four O_2 molecules to $O_2^{-\bullet}$. Reaction (3)— The four $O_2^{-\bullet}$ dismutate or decompose (rapidly) into two H_2O_2 molecules, reforming two molecules of O_2. Such reactions are enzymatically catalyzed by thylakoid-bound SODs. Reaction (4)—A complete degradation of two H_2O_2 further yields one molecule of O_2 and two H_2O, the latter reforming the H_2O originally oxidized at PSII, resulting in a net O_2 flux of zero. Noteworthy, if thylakoid bound ascorbate peroxidases and peroxiredoxines would eliminate the accumulation of H_2O_2, the whole process would end at Reaction (3) with production of H_2O in the WWC. This means that upon addition of external catalase (Cat), Reaction (4) would not commence. This would limit the O_2 flux ratio to Reaction (3) as shown in the scheme in Figure 1, which, however, was not the case in current experiments. At each of these four steps the stoichiometric ratio of O_2 produced to O_2 consumed varies, which we describe as the O_2 flux ratio (Figure 1, O_2 flux ratios). The O_2 flux ratio was quantified with MIMS by separating the two events from each other, that is the rate of PSII H_2O splitting reactions was measured by the production rate

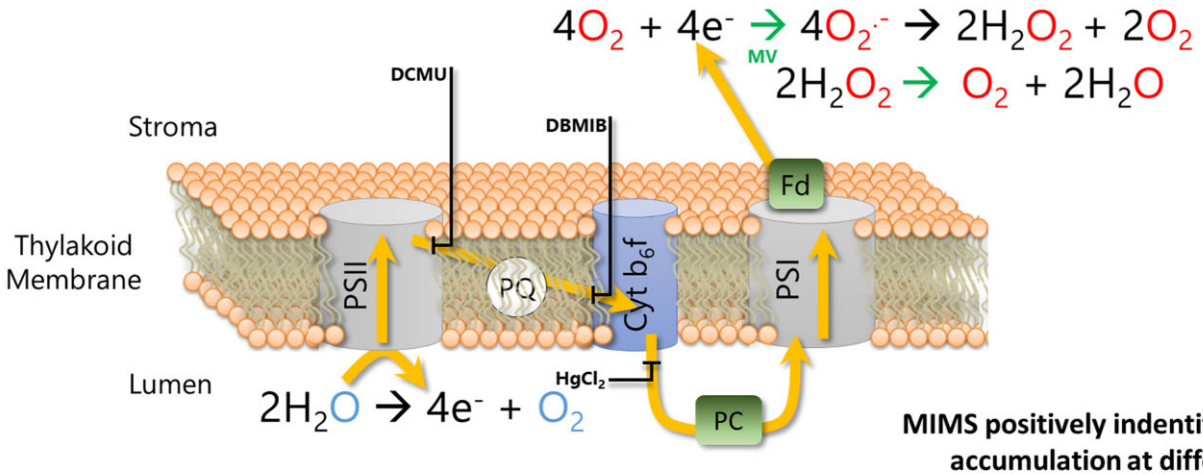

MIMS positively indentified H_2O_2 accumulation at different locations by O_2 Flux Ratio

Partial reactions of O_2 reduction, H_2O_2- accumulation and decomposition in isolated thylakoids

	$^{16}O_2$ Production : $^{18}O_2$ Consumption	
	$^{16}O_2$: $^{18}O_2$	Decimal
Reaction 1– $2H_2O \rightarrow O_2 + 4e^-$, at PSII donor side	1 : 0	1.00
Reaction 2– $4e^- + 4\ O_2 \rightarrow 4\ O_2^{\cdot-}$, at PSI acceptor side	1 : 4	0.25
Reaction 3– $4\ O_2^{\cdot-} \rightarrow$ (very rapid) $\rightarrow 2O_2 + 2\ H_2O_2$	1 : 2	0.50
Reaction 4– $2\ H_2O_2 \rightarrow$ (uncatalysed system = slow) $\rightarrow 2\ H_2O + O_2$	1 : 1	1.00
Reaction 5– No PSII activity, light induced O_2 consumption	0 : 1	0.00

Figure 1 Schematic description of O_2 reduction, H_2O_2 accumulation, and H_2O_2 decomposition cycle operating in isolated thylakoid membrane samples, highlighting labeled isotope reactions and the targets of specific PETC inhibitors, and catalysts, used in this study. Water oxidation at PSII generates a $^{16}O_2$, represented in blue font, and releases four electrons into the PETC, represented by yellow arrows. These four electrons reduce four artificially enriched $^{18}O_2$, represented in red font. According to the reactions presented at the top right, the superoxide is dismutated into H_2O_2 and finally back to H_2O, reproducing the H_2O originally oxidized but now containing a red, labeled O_2. This final reaction can be catalyzed by externally added catalase (Cat) in the isolated thylakoids, which instantly pushes the cycle to the end. Breaking the complete cycle into partial reactions (Reactions 1–4) provides a stoichiometric gas flux ratio to associate each step of the cycle back to the O_2 production to consumption ratio being measured with MIMS. Reactions 1 and 4 have the same ratio but are distinguished by the O_2 uptake component, occurring only with artificial acceptors. Three well-known inhibitors DCMU, DBMIB, and $HgCl_2$ are shown at the site of inhibition in electron transport chain that is the PQ-pool reduction at Q_B binding site, the PQ-pool oxidation at Cyt-b_6f and the plastoquinone reduction at Cyt-b_6f. Reaction 5 is a variant of the ratio, predicted from observations that DCMU blocks all water oxidation but samples were still able to consume O_2 in a light dependent manner, suggesting $^1O_2$ or organic peroxide formation. PQ, plastoquinone.

of the naturally abundant O_2 isotopolog (Figure 1, $^{16}O_2$, blue font), while O_2 reduction reactions were determined by the consumption rate of the artificially enriched heavy O_2 isotopolog (Figure 1, $^{18}O_2$, red font).

The key advantages of the first and second steps of our approach, compared with measuring net O_2 fluxes polarographically, are that (1) no assumptions are required to determine the number of electrons entering the PETC, (2) the 1:1 ratio of Reaction 4 is measurable, even if H_2O_2 is catalytically decomposed, and (3) it is possible to clearly observe when O_2 was consumed in the absence of electron transport, that is, to observe the 0:1 stoichiometry described in Reaction 5 (Figure 1), which results from lipid/protein peroxidation reactions such as those resulting from $^1O_2$ formation. As the third step in our approach, electron paramagnetic resonance (EPR) spin-trapping was applied to thylakoid samples under similar experimental conditions. This enabled us to directly infer the ROS formed at each location in the PETC, to support the observations and conclusions made with the MIMS data.

Results

Controlling ROS formation at PSI resulting from partial blockage of PETC

As described in Figure 1, application of specific inhibitors enables systematic segmentation of the PETC into discrete components. It was then possible to measure the site-specific ROS formation of each component with MIMS or EPR. However, the efficacy of each inhibitor to completely block the re-reduction of oxidized P700 ($P700^+$, special chlorophyll pair in PSI) had to be systematically confirmed via P700 spectroscopy, using a Dual PAM, under emulated experimental conditions (Figure 2), in order to avoid any artifacts during measurement of illuminated samples with EPR or MIMS from a still active PSI Mehler reaction. The oxidation of P700 was achieved through application of a

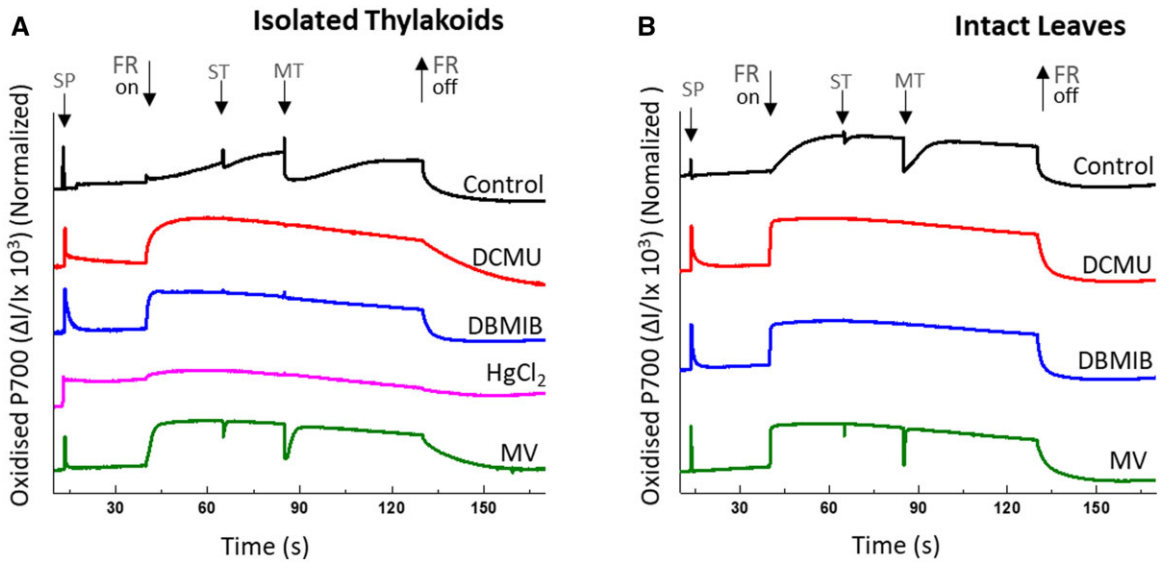

Figure 2 Comparison of site-specific inhibitors in blocking electron flow from PSII to PSI. Dark-adapted isolated thylakoids, or intact leaves, were exposed to a saturating pulse (SP) of actinic light. Following this, P700 re-reduction was measured under FR background illumination by firing strong actinic light (10,000 μmol photons m^{-2} s^{-1}) pulses for 50 μs (ST) and 50 ms (MT) on (A) isolated thylakoids equivalent to chlorophyll concentration of 80 μg chl mL^{-1} in measuring buffer containing the uncoupler NH_4Cl (5 mM) and (B) intact leaves. Leaves were infiltrated in darkness using water for the control sample. Inhibitors/modulators were used at 10 μM concentration, except for $HgCl_2$ used at 2 mg mL^{-1}. Representative curves averaged from minimum three to five biological replicates (n = 3).

background far red (FR) light (128 μmol photons m^{-2} s^{-1}) and following simultaneously the re-reduction of P700 by activation of the PSII catalyzed electron transfer for 50 μs (singleturnover, ST flash) and 50 ms (multiple turnover, MT) by exposure of strong actinic light pulses (10,000 μmol photons m^{-2} s^{-1}). The redox measurement and quantification of P700 in Dual PAM is based on strong absorption characteristics of oxidized P700 between 800 and 840 nm. A difference of transmittance between the 875 and 830 nm in darkness shows completely reduced P700. The calibrated kinetic signal of P700 is represented as $\Delta I/I \times 10^{-3}$ units. The following inhibitors were tested and used: (1) DCMU, as an inhibitor of PQ pool reduction, enabled PSII to be heavily reduced (Witt et al., 1968), (2) DBMIB, as an inhibitor of PQ oxidation by Cyt-b_6f, enabled complete reduction of PSII and the PQ pool (Bauer and Wijnands, 1974), and (3) $HgCl_2$, as an inhibitor of plastocyanin (PC) function, enabled reduction of PSII, PQ pool, and Cyt-b_6f (Kimimura and Katoh, 1972). Historically, DNP-INT has been used to block reduction of Cyt-f while enabling interaction of the low potential chain of Cyt-b_6f complex with plastosemiquinone, considered necessary for the formation of $O_2^{-\bullet}$ within the PQ-pool (Khorobrykh and Ivanov, 2002; Mubarakshina and Ivanov, 2010). However, in an attempt to maintain such dynamics between the PQ pool and Cyt-b_6f in isolated thylakoids and leaf discs, we observed that DNP-INT failed to completely block the reduction of PSI (Fitzpatrick et al., 2020). Hence, $HgCl_2$ was considered the best available alternative. Although $HgCl_2$ has been reported to have multiple inhibitory effects on photosynthetic apparatus (Carpentier, 2001), we observed strong PSII activity in isolated thylakoid membranes in the presence of $HgCl_2$ under both growth light (GL) and high light (HL) (see Supplemental Figure S1).

Freshly prepared isolated thylakoid (Figure 2A) and intact leaf (Figure 2B) samples from Arabidopsis were incubated in darkness with 10 μM DCMU, 10 μM DBMIB, or 2 mg mL^{-1} $HgCl_2$ (we found $HgCl_2$ toxic to intact leaves so this inhibitor was applied only for isolated thylakoid samples). As negative controls for blocking PSI activity, 10 μM methyl viologen (MV; catalyst of O_2 reduction at PSI acceptor side) and untreated control samples were also measured. During the preceding dark incubation, a single saturating pulse (SP) of actinic light revealed an overall capacity of each sample to rapidly oxidize P700 followed by fast re-reduction in all samples except for the $HgCl_2$-treated thylakoids. Subsequently, the electrons released from water by PSII into the PETC by actinic light pulses transiently reduced $P700^+$ in both sets of untreated control samples (Figure 2, A and B, black traces), evidenced by the pulse length-dependent decrease, or "dip" of the $P700^+$ signal, before being fully re-oxidized by the continuous FR background light (Tiwari et al., 2016). In contrast, no transient dip was observed in the $P700^+$ signal when thylakoid samples were treated with DCMU, DBMIB, or $HgCl_2$ (Figure 2A, red, blue, and pink color traces), or in leaves treated with DCMU or DBMIB (Figure 2B, red and blue traces). This confirmed that these inhibitors blocked all electron transport from PSII to PSI. Uniquely, $HgCl_2$ blocked the re-reduction of $P700^+$ in isolated thylakoid samples following the actinic light pulse in the initial dark phase of the measurement (Figure 2A, pink trace). This was consistent with $HgCl_2$ targeting the function

of PC, which was then severely restricted in its capacity to deliver electrons to $P700^+$ throughout the rest of the measurement. Samples infiltrated with MV (Figure 2, A and B, green traces) exhibited clear actinic light dependent dips. However, due to the accelerated rate of re-oxidation produced by the artificial PSI acceptor, and catalyst of $O_2^{-\bullet}$ formation, the "dips" following ST and MT pulses were "narrowed" compared with the control samples (Figure 2, A and B, black traces,) in which electrons took longer to find an acceptor.

O_2 flux ratio measured with MIMS positively identified H_2O_2 accumulation in thylakoid samples

Freshly prepared thylakoid samples were illuminated at a relatively low light intensity, equivalent to GL (120 µmol photons m^{-2} s^{-1}), to minimize $^1O_2$ formation and to verify that H_2O_2 accumulation results in a 1:2 O_2 flux ratio (Figure 1) in MIMS measurements (Figure 3, A–G). To ensure that the O_2 flux ratios were calculated based on light-dependent O_2 fluxes, the background dark rate of O_2 consumption (also observed in Furbank and Badger (1983) was offset to zero. Control samples (Figure 3A) produced O_2 in a relatively stable manner across the 3 min of illumination, at a rate of ~2.5 µmol mg chl^{-1} h^{-1}. The simultaneous rate of O_2 consumption was less stable, exhibiting a steady decrease in the integrated rate over the 3 min of illumination. However, the initial O_2 consumption rate of ~5.0 µmol mg chl^{-1} h^{-1} was double the initial O_2 production rate, resulting in an O_2 flux ratio of 1:2, consistent with accumulation of H_2O_2 (Figure 1). The addition of Cat (700 unit/mL^{-1}) to rapidly degrade any H_2O_2 formed did not drastically affect the rate or stability of O_2 production (Figure 3B). However, it decreased the absolute rate of O_2 consumption so that it matched the O_2 evolution rate, resulting in the 1:1 O_2 flux ratio expected in the absence of H_2O_2 accumulation (Figure 1). It is clear that when H_2O_2 accumulates, the rate of O_2 consumption is greater than the rate of O_2 evolution (Figure 3, A and C) (red line is a greater magnitude than the blue line and net rate shown with a gray line is negative). In contrast, when the accumulation of H_2O_2 is excluded by the addition of Cat (Figure 3, B and D) or in samples excluding PSI function (Figure 3, E–G), we clearly observed that O_2 consumption cannot substantially exceed O_2 production, as any H_2O_2 formed was immediately decomposed, re-releasing the $^{18}O_2$.As a positive control for H_2O_2 accumulation, and to simultaneously test the sample's acceptor side limitation at PSI, 10 µM MV was added to thylakoid samples. The O_2 evolution

rate increased to 12.5 µmol O_2 mg chl^{-1} h^{-1} and the initial O_2 consumption rate of 25.0 µmol O_2 mg chl^{-1} h^{-1} reproduced the O_2 flux ratio of 1:2 observed in control samples (Figure 3C, observe change in *y*-axis scale). This result verified that control samples illuminated at GL were PSI acceptor limited; therefore, all components of the thylakoid membrane were heavily reduced during illumination. The addition of Cat to MV-treated thylakoid samples (Figure 3D) replicated the effects of Cat added to control thylakoids, reproducing a 1:1 O_2 flux ratio with no effect on the rate of O_2 production. The strong negative O_2 consumption rate following illumination, both in control and amplified in MV treated samples, suggested that the declining O_2 consumption rate during illumination was a product of $^{18}O_2$ release from an accumulated H_2O_2. This was supported by the observation that the sum of the O_2 consumption rate at the end of the light period and the negative rate at the beginning of the dark period approximated the initial O_2 consumption rate in untreated control and MV samples (for a more detailed explanation of interpreting time-resolved gas flux transients, and how the negative O_2 consumption burst has been interpreted as the decomposition of an accumulated H_2O_2 pool, refer to Supplemental Figure S2). In the summary bar chart of the O_2 flux ratios (Figure 3H), it can be seen that the control and MV treated samples exhibited an O_2 flux ratio of 1:2. Conversely, in samples where Cat precluded H_2O_2 accumulation an O_2 flux ratio of 1:1 was observed. Hence, MIMS was able to discriminate between isolated thylakoid samples in which H_2O_2 was accumulated from those in which the H_2O_2 was rapidly decomposed.

MIMS confirms that O_2 reduction at PQ-pool and Cyt-b_6f cannot accumulate H_2O_2

To compare the site-specific capacity of heavily reduced PETC components upstream of PSI to generate ROS and accumulate H_2O_2 in vitro, we measured the O_2 flux ratios of freshly isolated thylakoid samples incubated with 10 µM DCMU, 10 µM DBMIB, or 2 mg mL^{-1} $HgCl_2$. Based on the results of MV addition to isolated thylakoids, discussed above, we were confident that components within the PETC were heavily reduced at GL irradiance. Incubation with DCMU clearly impaired all O_2 production (Figure 3E) and although noisy, O_2 consumption was minimal. In contrast, samples incubated with DBMIB exhibited strong O_2 production by water oxidation at the initiation of illumination, in the absence of commensurate O_2 consumption. This resulted in an initial O_2 flux ratio of 1:0 (Figure 1, Reaction 1), consistent with DBMIB accepting electrons from PSII as reported previously (Lozier and Butler, 1972). The rate of O_2 production peaked; presumably as available DBMIB was fully reduced and then slowed as O_2 consumption became the primary electron sink (more evidence that samples were acceptor-limited). The steady-state rate of O_2 production and consumption of ~1.0 µmol O_2 mg chl^{-1} h^{-1} (Figure 3F) comprised an O_2 flux ratio of 1:1. This ratio matched the addition of Cat to control and MV treated thylakoid samples. According to the results of a DBMIB concentration–response curve, the integrated area of the O_2 evolution peak was DBMIB concentration-dependent (r^2 of 0.99) while the steady-state rate following the peak was DBMIB concentration-independent (Supplemental Figure S3). This result thus suggested that DBMIB was not acting as a

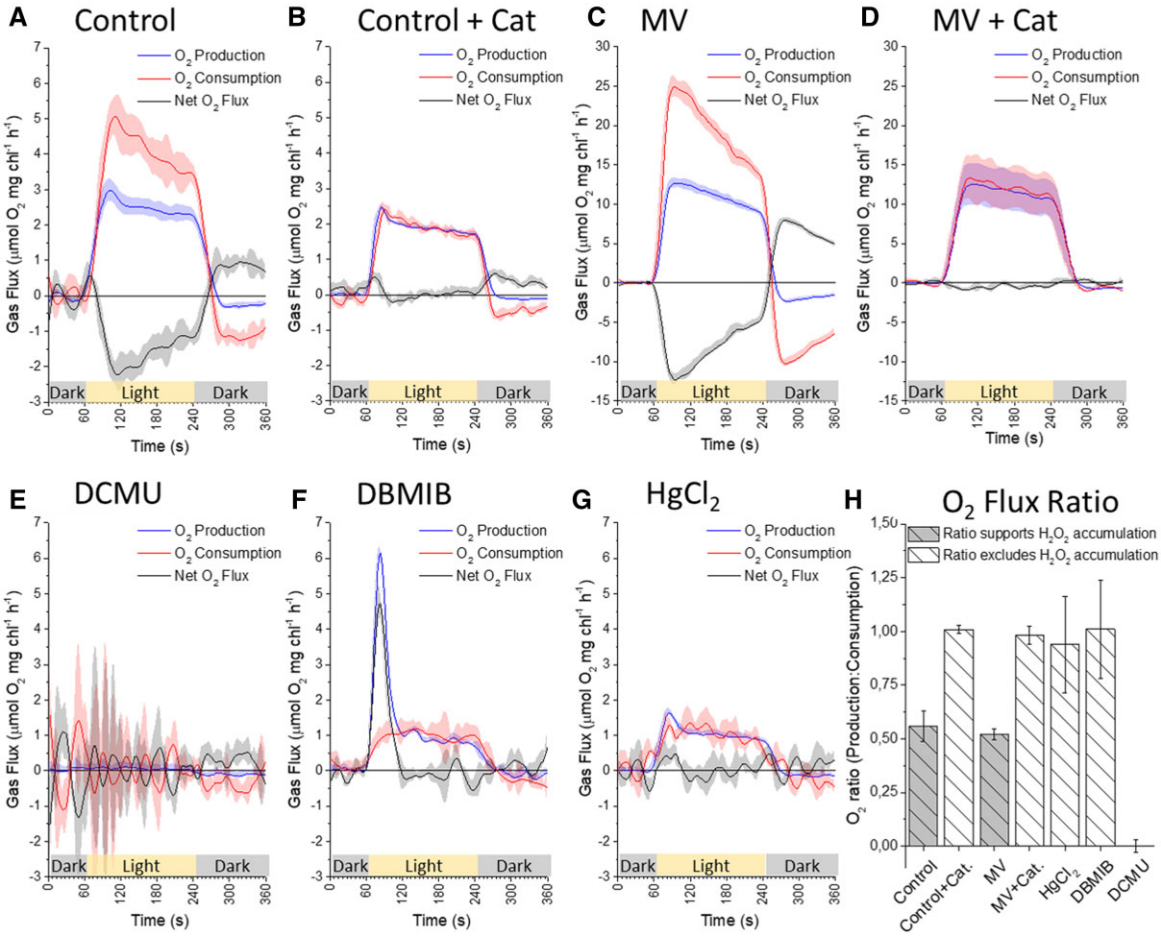

Figure 3 Integrated rates of $^{16}O_2$ production and $^{18}O_2$ consumption by isolated thylakoid samples, measured simultaneously at 120 µmol photons m^{-2} s^{-1} with MIMS. Illumination of samples represented by yellow bar with gray representing darkness. Curves A, untreated control; B, untreated control + Cat; C, 10 µM (MV), D, 10 µM MV + Cat (observe increased scale for c and d), E, 10 µM DCMU, F, 10 µM DBMIB and G, 2 mg mL^{-1} $HgCl_2$ are the product of averaging minimum three replicates plotted with standard error. H, The ratios of O_2 production to consumption rates were calculated as described in text and plotted as a decimal value to highlight conditions in which H_2O_2 could accumulate, based on the stoichiometry of partial reactions from O_2 reduction to water formation again. All measurements were performed in measurement buffer containing the uncoupler NH_4Cl (5 mM). All curves are an average of minimum three representative replicates (n = 3) plotted with standard error (±SE).

redox intermediate in the steady-state O_2 consumption pathway. Incubating thylakoids with $HgCl_2$ (Figure 3G) produced a very similar PSII activity as that in DBMIB samples, exhibiting a steady-state rate of O_2 production ~1.0 µmol O_2 mg chl^{-1} h^{-1} and a 1:1 O_2 flux ratio. Importantly, the lack of a large initial peak in O_2 production supported the conclusions drawn from the DBMIB concentration–response curve (Supplemental Figure S3). The small initial peak in O_2 production observed with $HgCl_2$ was also evident in control samples with and without Cat (Figure 3, A and B) but absent from DCMU curves, suggesting it was the product of reducing a small intrinsic pool of acceptors between PSII and PSI, likely the PQ pool.

The fact that $HgCl_2$ and DBMIB samples exhibited almost identical steady-state rates and a 1:1 O_2 flux ratio at GL supported the contention that a pathway to O_2 reduction operates within the thylakoid membrane. While this pathway upstream of PSI exhibited a smaller capacity to reduce O_2 compared to the PSI Mehler reaction, it clearly supports PSI independent steady-state turnover of PSII. PTOX may be a candidate to explain such a pathway, reducing O_2 to H_2O with reductant from PQH_2 (Cournac et al., 2000). In an effort to control for PTOX function, we repeated DBMIB measurements in the presence of the widely used PTOX inhibitors *n*-propyl gallate or octyl gallate (Cournac et al., 2000). Unexpectedly in our measurements, both treatments enhanced O_2 production (PSII activity) and O_2 consumption, even in the presence of DCMU (Supplemental Figure S4, with short discussion of these experiments). We did not investigate this result further, concluding that based on analysis of the P700 kinetics of isolated thylakoids (Figure 2A) and the O_2 Flux ratios of thylakoid samples (Figure 3H), H_2O_2 can only accumulate in the thylakoid membrane if electrons are able to reach PSI.

Increasing the redox and excitation pressure highlighted separate ROS pathways within the thylakoid membrane in vitro

To test the impact of increased excitation and redox pressure on the results described above, we repeated all MIMS measurements with inhibitors using HL illumination (900 µmol photons m^{-2} s^{-1}) (Figure 4). The untreated control samples increased rates of O_2 production and consumption to ~5 and 10 µmol O_2 mg chl^{-1} h^{-1}, respectively (Figure 4A), while the 1:2 O_2 flux ratio was maintained. We assured that relatively low rates observed were a result of the lack of electron acceptors in isolated thylakoids (no externally added ferredoxin [Fd]) and the absence of extra SOD in our experiments. Contrasting to untreated control thylakoids, the DCMU response was markedly different at higher illumination. The dosage required to fully impair PSII function increased to 50 µM and a strong light-dependent, Cat independent, O_2 consumption was observed at a rate of ~1.5 µmol O_2 mg chl^{-1} h^{-1} (Figure 4, B and F), consistent with previously published observations (Khorobrykh et al., 2011). The O_2 flux ratio of 0:1 in DCMU-treated thylakoids was consistent with activity of Reaction 5 (Figure 1), suggesting peroxidation of lipids and membranes via formation of $^1O_2$ and/or organic peroxides (Khorobrykh et al., 2011), in the absence of water splitting at PSII. Addition of Cat had no effect on the measured rates (Figure 4F) confirming that H_2O_2 accumulation was not behind the observed O_2 consumption. This is in line with findings, based on the use of the fluorescent biosensor HyPer2, that PSII cannot generate H_2O_2 in the presence of DCMU (Exposito-Rodriguez et al., 2017). Increased irradiance also affected the DBMIB and $HgCl_2$ treatments. Steady-state O_2 production by DBMIB treated samples increased by ~50%, from 1.0 up to 1.5 µmol O_2 mg chl^{-1} h^{-1} (Figure 4C), while it increased three-fold in the $HgCl_2$ samples, from ~1.0 to 3.0 µmol O_2 mg chl^{-1} h^{-1} (Figure 4D). However, O_2 consumption rates in both treatments increased by a larger relative amount than O_2 production, shifting the apparent O_2 flux ratio toward 1:2 (Figure 4E). Although, based on the O_2 flux ratio, this suggested that H_2O_2 was accumulating within the thylakoid membrane, we observed that the rate of O_2 consumption in DBMIB samples was insensitive to Cat (Supplemental Figure S5A, we could not measure $HgCl_2$ samples with Cat due to the toxicity of Hg^{2+} for the Cat enzyme). We suspect that the isolated thylakoid samples experience strong acceptor side limitation at PSII. This was exacerbated by the higher irradiance which increased the probability of chlorophyll triplet states and therefore $^1O_2$ formation. The $^1O_2$ associated lipid/membrane peroxidation was enhanced by the HL treatment, resulting in a strong background rate of O_2 consumption not associated with electron transport or $O_2^{-\bullet}$ formation, previously defined as DCMU insensitive O_2 consumption (Furbank and Badger, 1983).

This interpretation was supported when we tested MV + Cat at HL, in which a small Cat insensitive O_2 consumption was also observed (Supplemental Figure S5B). In order to account for the contribution of $^1O_2$ formation in calculating the absolute O_2 flux ratios of DBMIB and $HgCl_2$ samples, the DCMU + Cat rates were directly subtracted from the DBMIB and $HgCl_2$ results (Figure 4, G and H). Resultant curves from both DBMIB and $HgCl_2$ treatments were almost identical to those measured at GL, excluding the slight increase in steady-state gas fluxes. Both exhibited an O_2 flux ratio of ~1:1 (Figure 4E), further supporting that H_2O_2 cannot accumulate within the thylakoid membrane at either PSII, the PQ pool, or Cyt-b_6f complex. This conclusion was further reinforced by the insensitivity to Cat of the HL enhanced O_2 uptake of DBMIB-treated thylakoid samples (Supplemental Figure S5A).

EPR spin trapping data, consistent with conclusions from in vitro MIMS measurements, support the function of PTOX

To test conclusions relating to ROS formation in the PETC based on MIMS measurements, we next applied EPR spin trapping to isolated thylakoid samples. We used 5-(diisopropoxyphosphoryl)-5-methyl-1-pyrroline-*N*-oxide 2-diisopropylphosphono-2-methyl-3,4-dihydro-2H-pyrrole-1-oxide (DIPPMPO), a more lipophilic spin trap with higher sensitivity and greater adduct stability for $O_2^{-\bullet}$ (DIPPMPO-OOH), $OH^{-\bullet}$ (DIPPMPO-OH), and carbon-centered adducts (DIPPMPO-R) than other commonly used spin traps like DMPO (Villamena, 2017). Isolated thylakoids were incubated with DIPPMPO in darkness for 5 min, before sample illumination with actinic light for 3 min at 150 µmol photons m^{-2} s^{-1}. Samples were then centrifuged and the supernatant transferred into an EPR capillary for measurement, while the pellet was discarded. To compare the relative capacity for ROS formation at different locations within the PETC compared with untreated controls, the inhibitors DCMU and $HgCl_2$ were applied across a series of measurements with MV included as a positive control for enhanced $O_2^{-\bullet}$ adduct formation. Based on our MIMS results on redox activity of DBMIB (Figures 3F and 4, C and G), we excluded DBMIB from EPR measurements as it is also known to alter the redox potential of the iron–sulfur clusters of PSI and Cyt-b_6f complex (Malkin, 1981), thus possibly producing artifacts and interference in EPR spin trapping of ROS.

To control putative background EPR signals, potentially arising from DIPPMPO incubation with isolated thylakoids and the inhibitors, the EPR response of each sample was measured after 5 min of dark incubation. No EPR signal was produced in darkness (Figure 5A). Illumination of the spin trap with control thylakoids generated a clear spin trap-ROS adduct signal (Figure 5B, black trace) which increased two- to three-fold through addition of MV (Figure 5B, purple trace). We performed a simulation fitting of the experimental EPR spectra to figure out what proportion of different radicals are present in it. Auto simulation was performed by Winsim application using previously reported values of hyperfine coupling constants for DIPPMPO adducts (Chalier and Tordo, 2002), setting a 1% limit for *g*-value and

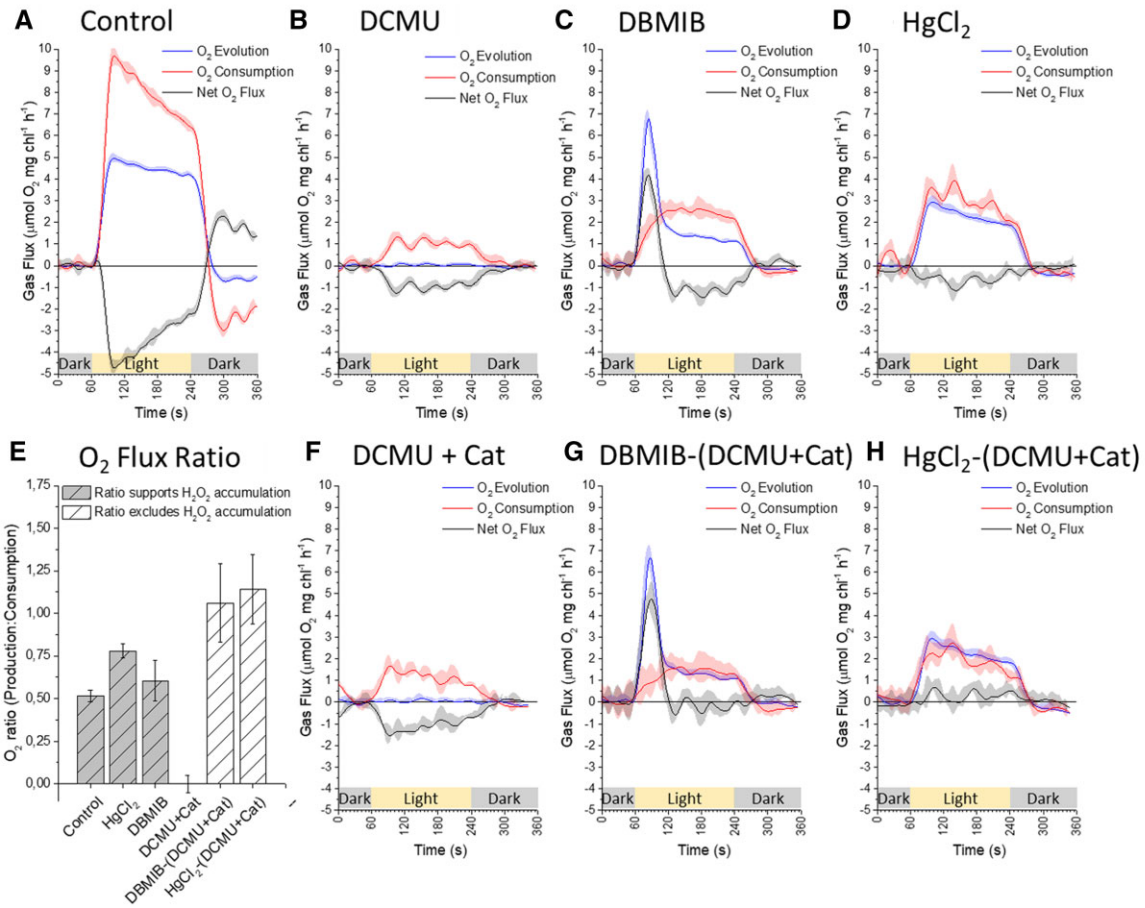

Figure 4 Integrated rates of $^{16}O_2$ production and $^{18}O_2$ consumption by isolated thylakoid samples, measured simultaneously at 900 µmol photons m^{-2} s^{-1} with MIMS. Illumination of samples represented by yellow bar with gray representing darkness. A, untreated control, B, 50 µM DCMU C, 10 µM DBMIB, and D, 2 mg mL^{-1} $HgCl_2$. O_2 consumption rates increased more than O_2 production rates in all inhibited samples, compared with measurements at 120 µmol photons m^{-2} s^{-1}. F, 50 µM DCMU + Cat suggests $^1O_2$ formation as a likely reason for increased O_2 consumption, subsequently this curve was subtracted from both DBMIB and $HgCl_2$ curves resulting in (G) DBMIB-(DCMU + Cat) and (H) $HgCl_2$-(DCMU + Cat). E, Plotting O_2 production to O_2 consumption ratios from all curves highlights that subtraction of O_2 consumption associated with peroxidation of lipids, proteins, and membranes by $^1O_2$ resulted in the return of O_2 flux ratios that exclude the accumulation of H_2O_2. All curves are an average of minimum three representative replicates (n = 3) plotted with standard error (±SE). All measurements of isolated thylakoids were performed in measurement buffer containing the uncoupler NH_4Cl (5 mM).

hyperfine coupling constants but enabling automatic adjustment for other parameters during fitting. The best fit simulated spectrum of DIPPMPO radical is obtained (Figure 5C) for an experimental spectrum of untreated control thylakoids (Figure 5B, upper trace). It contained ∼73% $O_2^{-\bullet}$ adduct (DIPPMPO-OOH), 18% $OH^{-\bullet}$ (DIPPMPO-OH), and 9% carbon-centered adduct (DIPPMPO-R). Variation of 5%–10% was observed in the contribution of superoxide and hydroxyl adducts between biological replicates.

The addition of DCMU decreased the measured spin-trap signal by 90% compared with untreated controls (Figure 5B). A very weak signal in DCMU treated thylakoids comprised ∼65% carbon-centered radicals and only small contributions were observed from $O_2^{-\bullet}$ and $OH^{-\bullet}$ adducts (Figure 5B, blue trace). This was consistent with the 0:1 O_2 flux ratio (Figure 1, Reaction 5) observed in MIMS data (Figure 4B) and the peroxidation of lipids and membranes via formation of $^1O_2$ and/or organic peroxides (Khorobrykh et al., 2011). The addition of $HgCl_2$ reduced the adduct signal up to 95% compared with the untreated control samples (Figure 5B, green trace), despite MIMS data showing that $HgCl_2$ only slowed PSII O_2 evolution, and associated O_2 consumption, by ∼40% (Figures 3G and 4H). While the O_2 dynamics strongly suggest that electrons produced through oxidation of water at PSII were accepted by O_2, the lack of $O_2^{-\bullet}$ adduct formation infers enzymatic reduction of O_2 to water, without formation of ROS. Such a pathway is reminiscent of the flavodiiron proteins functional at the PSI acceptor side in lower-order phototrophs and gymnosperms (Ilík et al., 2017) and makes it conceivable that PTOX performs a similar function in flowering plants. The data are also consistent with function of the theorized PQH_2/PQH^- mechanisms for formation and quenching of $O_2^{-\bullet}$ (Khorobrykh and Tyystjärvi, 2018). However, spin-traps are notorious for their

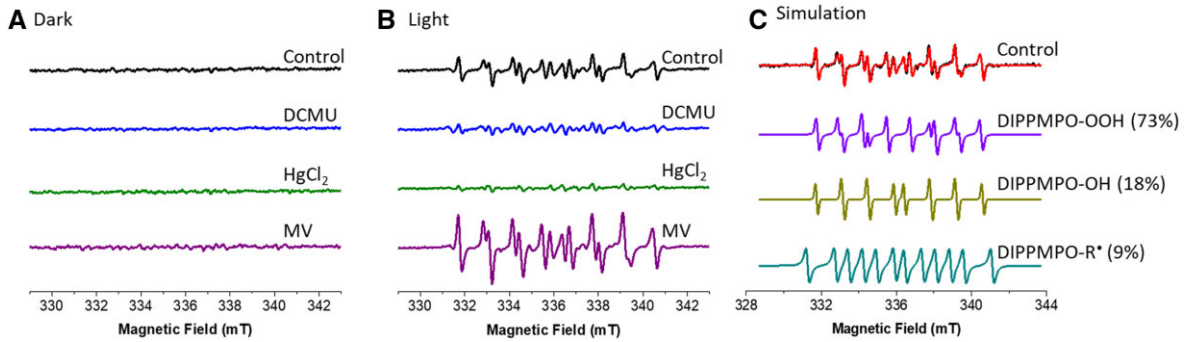

Figure 5 Light-induced superoxide formation in isolated thylakoids. Superoxide was measured by spin trapping with DIPPMPO (A) in the dark and (B) after 3 min of illumination with white light (150 μmol photons m^{-2} s^{-1}). Typical spectra of DIPPMPO-OOH with hyperfine splitting constants (cis a_P 4.968 mT, a_N 1.314 mT, a_H 1.102 mT; trans a_P 4.95 mT, a_N 1.301 mT, a_H 1.022 mT), DIPPMPO-OH (a_P 4.659 mT, a_N 1.414 mT, a_H 1.339 mT) and DIPPMPO-R (*a*P 4.59 mT, *a*N 1. 491 mT, *a*H 2.22 mT) adducts were measured in the presence of DCMU (Q_B–site inhibitor), $HgCl_2$ (PC inhibitor), and MV (Catalyst of O_2 reduction at PSI). C, Simulated spectra of the experimental spectrum of control thylakoids from (B), Light upper trace consisting of different proportion of each DIPPMPO-OOH, DIPPMP-OH, and DIPPMPO-R are shown. Thylakoids were isolated from 6-week-old plants, grown under constant light of 120 μmol photons m^{-2} s^{-1} with dark and light cycle of 16/8 h. Thylakoids equivalent to 150 μg chl mL^{-1} were illuminated with actinic light (150 μmol photons m^{-2} s^{-1}) in the presence of 50 mM DIPPMPO, 100 μM desferal, and 50 mM Hepes–NaOH (pH 7.5) with each electron transfer modulator DCMU (10 μM), $HgCl_2$ (2 mg/150 μg chl), and MV (10 μM). EPR settings were microwave frequency 9.41 GHz, center field 336.2 mT, field sweep 15 mT, microwave power 5 mW, modulation frequency of 100 kHz, modulation width of 0.05 mT, sweep time 60 s. A minimum three to five independently isolated thylakoid samples (n = 3) were used for the final spectra, and five accumulations were recorded from each sample.

inefficiency at penetrating the membranes, making this data difficult to interrogate further. Despite this, the suppression of the EPR spin-trap signal (Figure 5B), in conjunction with the 1:1 O_2 flux ratio measured with MIMS (Figures 3G and 4H), rules out the accumulation of H_2O_2 in $HgCl_2$-treated thylakoid samples. As $HgCl_2$ enabled the reduction of all components upstream of PSI, these data offer robust evidence that stable accumulation of H_2O_2 requires PSI activity.

Detecting photosynthetic H_2O_2 accumulation via O_2 stoichiometry in leaf discs

To test the applicability of our in vitro findings, we developed a MIMS methodology to estimate O_2 flux ratios in vivo (Arabidopsis leaf discs), under similar conditions to those tested with isolated thylakoids. As the primary terminal electron acceptor in leaves is CO_2 and mitochondrial respiration is a large contributor to O_2 consumption, it was not possible to simply divide the gross O_2 production rate by the gross O_2 consumption rate. Alternatively, we estimated the O_2 flux ratio associated specifically with the steady-state WWC determined in the absence of photorespiration. Assuming a 1:1 ratio between $^{16}O_2$ evolution and $^{13}CO_2$ (artificially enriched) fixation by Rubisco during oxygenic photosynthesis, we determined the difference between the production of electrons at PSII and the consumption of electrons by the Calvin–Benson–Bassham (CBB) cycle. This difference provided an upper limit of $^{16}O_2$ production specifically linked to the WWC. The rate of $^{18}O_2$ consumption associated with the Mehler reaction was then determined by subtracting the rate of $^{12}CO_2$ produced by mitochondrial respiration, from the gross rate of $^{18}O_2$ consumption (assuming a 1:1 ratio between CO_2 production and O_2 consumption during aerobic mitochondrial respiration). By simultaneously measuring the fluxes of four stable isotopes, representing isotopologs of both O_2 and CO_2, we could estimate the steady-state rate of O_2 production and O_2 consumption associated specifically with the WWC and hence, estimate the in vitro and in vivo O_2 flux ratio according to the scheme in Figure 1.

Arabidopsis leaf discs (12.5 mm in diameter) were floated overnight in near darkness on water containing 10 μM DCMU, 10 μM MV, or 10 μM DBMIB (or plain water—untreated control), then sealed into the MIMS cuvette and purged with air scrubbed of all $^{12}CO_2$ (Soda Lime, Li-Cor USA). To this 3% $^{13}CO_2$ and 2% $^{18}O_2$ were injected by volume (total O_2 ~21%). After a few minutes darkness to ensure isotopic equilibrium throughout the sample, data acquisition was initiated. An illumination protocol of 3 min darkness, 5 min at GL, 5 min at HL, and 3 min darkness was applied. In the data, all samples exhibited an apparent "peak" of $^{18}O_2$ production during transition from GL to HL, and $^{18}O_2$ uptake following transition from HL to darkness. This trend was also observed in the blank control measurements (Supplemental Figure S6) indicating that it was an artifact, potentially a light effect on the membrane. To avoid this artifact and emphasize the steady-state results in the main panels, the integrated gas flux rates versus time (Figure 6, A, B, D, and E) are displayed with breaks in the *x*-axis. For reference, the inset figures display the full curves. All rates used to calculate the O_2 flux ratios (Figure 6F) are based on the averaged steady-state fluxes measured from minimum three biological replicates. These values are

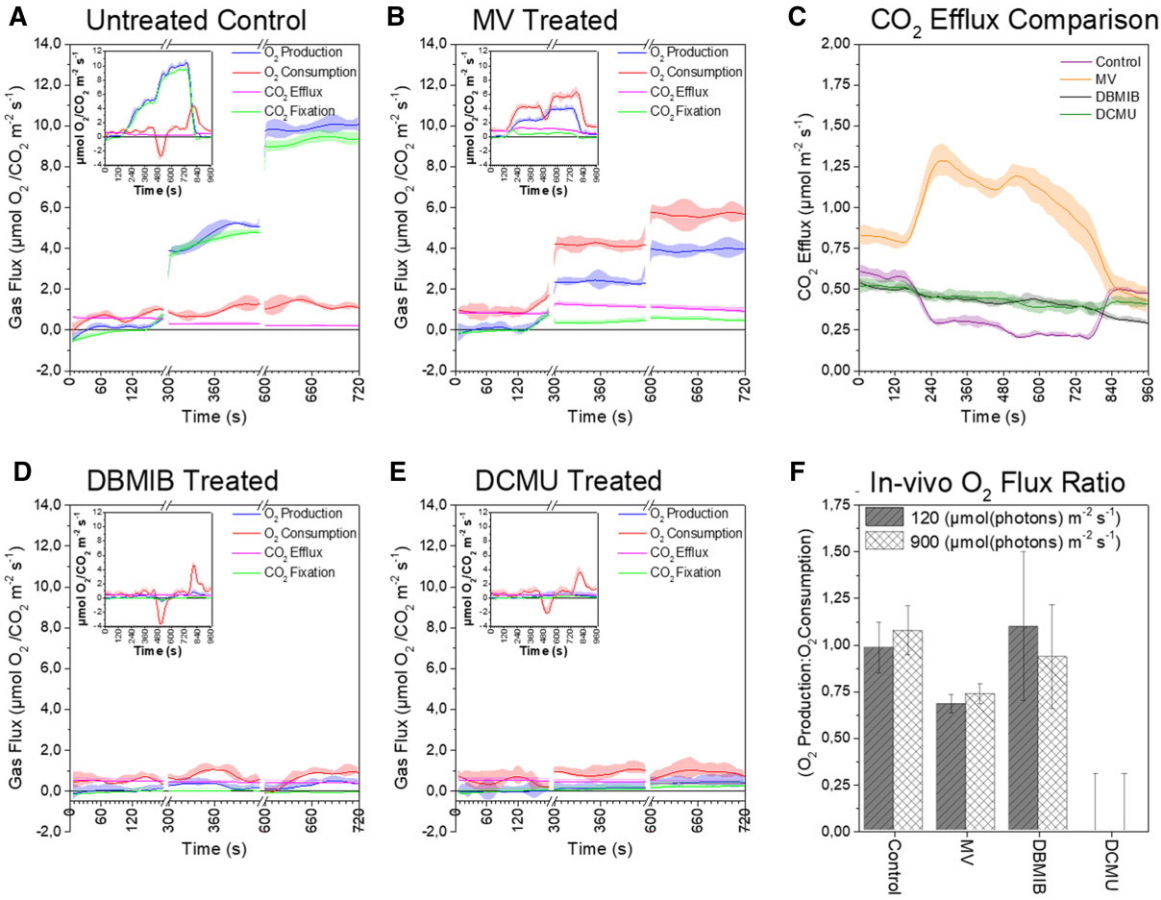

Figure 6 The integrated rates versus time of O_2 and CO_2 fluxes from intact leaf discs measured at three different light conditions. Rate versus time plots of (A) control, (B) MV, (D) DBMIB, and (E) DCMU infiltrated leaf discs. Inset shows complete curves and the main figure highlights steady-state rates across the dark and two light intensities GL = 120 (from 300 to 600 s) and HL = 900 (600–720 s) µmol photons m^{-2} s^{-1}, respectively. For direct comparison, part C shows CO_2 efflux rates (mitochondrial respiration) from the four treatments. F, O_2 flux ratio associated with Mehler reaction calculated as described in text. All curves average of minimum three representative replicates (n = 3) plotted with standard error (±SE). The apparent mismatch between activation of light and photosynthetic activity is a result of the integration of rates over time required to minimize noise and allowing a focus on steady-state rates.

presented as a table in the supplementary data (Supplemental Table S1).

Untreated control leaf discs (Figure 6A) performed as expected in a high CO_2 environment. Rates of O_2 production and CO_2 fixation (Figure 6, blue and green curves) were strongly related across all irradiances. The $^{12}CO_2$ efflux generated by mitochondrial respiration apparently decreased in association with increasing irradiance (Figure 6, A–E, pink line, Figure 6C, highlighted by purple line). This result was likely a product of CO_2 re-fixation (Busch et al., 2013), as such dark respiration was assumed to be constant when calculating the in vivo O_2 flux ratio from untreated control discs, as concluded by Farquhar and Busch (2017). The rate of O_2 production providing electrons used specifically in the Mehler reaction of control discs was estimated at 0.4 ± 0.3 and 0.7 ± 0.6 µmol O_2 m^{-2} s^{-1} at GL and HL, respectively. This matched the estimated rate of Mehler O_2 consumption of 0.4 ± 0.1 and 0.6 ± 0.4 µmol O_2 m^{-2} s^{-1} at GL and HL.

The resulting in vivo O_2 flux ratio of ∼1.0 (GL = 1.0 ± 0.1, HL = 1.1 ± 0.1) discounted accumulation of H_2O_2, as expected with an elevated CO_2 atmosphere. Despite differences in methodology, these rates compare well with previous MIMS-based estimates of Mehler-specific O_2 consumption under similar conditions (Mubarakshina and Ivanov, 2010).

The DBMIB treatment completely impaired $^{13}CO_2$ fixation (Figure 6D, green line) and had no effect on $^{12}CO_2$ efflux (Figure 6C, black line). However, light-dependent O_2 production was evident and it corresponded with an increase in the rate of O_2 consumption above that required for mitochondrial respiration. This result supports the function of an O_2 reduction pathway within the thylakoid membrane, observed in vitro, and the calculated O_2 flux ratio of ∼1.0 (GL = 1.1 ± 0.4 and HL = 0.9 ± 0.3) reinforced the in vitro conclusions that H_2O_2 cannot accumulate within the reduced PQ pool. The DBMIB dependent O_2 production "peak" was not observed in the leaf discs, potentially due to chlororespiration during dark incubation preceding the measurements that may have fully reduced all DBMIB in the samples before illumination. Contrasting the earlier

experiments, DCMU infiltration was not completely effective, although it severely impaired O_2 production during illumination (Figure 6E). However, this O_2 production was matched by commensurate CO_2 fixation during illumination (GL = 0.1 ± 0.06, HL = 0.2 ± 0.2 μmol m^{-2} s^{-1}). Importantly, the illuminated O_2 consumption rate doubled from a dark rate of 0.4 μmol O_2 m^{-2} s^{-1} to ~0.8 μmol O_2 m^{-2} s^{-1}. In the absence of any change to the respiratory CO_2 efflux (Figure 6C, green trace) and with all PSII activity accounted for by CO_2 fixation, the light-dependent O_2 consumption was most likely a product of $^1O_2$ formation and associated peroxidation of lipids, proteins, and membranes. The calculated O_2 flux ratio of zero (Figure 6F) was in-line with our in vitro MIMS and EPR results and in agreement with published literature that H_2O_2 cannot accumulate at PSII in the presence of DCMU (Exposito-Rodriguez et al., 2017).

As a final positive control to test the methodology in estimating H_2O_2 accumulation, we infiltrated leaf discs with MV. In leaf discs, MV competes with CO_2 fixation reactions for reductant at PSI, impairing rates of CO_2 fixation compared with untreated control discs. The accumulation of ATP that would otherwise be used in the CBB cycle limits the supply of phosphate for further ATP production. The subsequent impairment of ATP-synthase results in the accumulation of a strong proton gradient across the thylakoid membrane, which impairs O_2 production and likely results in a counterintuitively reduced PQ pool as previously described (Shapiguzov et al., 2020). The illuminated rate of O_2 consumption in MV treated leaf discs was approximately two-fold the rate of O_2 production, suggesting the accumulation of H_2O_2 (Figure 6B). However, in darkness, MV approximately doubled the $^{12}CO_2$ efflux rate associated with mitochondrial respiration compared with all other samples (Figure 6C, orange line), as observed by Scarpeci and Valle (2008). Uniquely for the MV treated samples, the $^{12}CO_2$ efflux rate was further enhanced by illumination. Assuming this was due to mitochondrial respiration with a 1:1 respiratory quotient accounted for a substantial portion of the increase in O_2 consumption. This observation was only possible due to our application of the $^{13}CO_2$ offset method, which enabled an accurate O_2 flux ratio of 0.7 ± 0.05 to be determined at both GL and HL. This ratio supports the formation and accumulation of some photosynthetically derived H_2O_2, as more O_2 was consumed than produced by PSII. However, the ratio also suggests that ROS scavenging components associated with the WWC were able to manage approximately half of the H_2O_2 produced in the presence of MV, at the impaired rates of PSII activity. Although the signal-to-noise ratio of this in vivo method could not discriminate subtle events, the in vivo data broadly supported the in vitro conclusions that (1) H_2O_2 could not accumulate at PSII (2) an O_2 reduction pathway operates in the presence of DBMIB which precludes the accumulation of H_2O_2. In addition, application of $^{13}CO_2$ to discriminate mitochondrial respiration from CO_2 fixation by the CBB cycle unexpectedly revealed a light-dependent stimulation of mitochondrial respiration in MV treated leaf discs, which we examined further.

Functional evidence suggests that H_2O_2 accumulation induces cooperation between chloroplasts and mitochondria

Infiltration with MV resulted in a light-dependent increase in mitochondrial $^{12}CO_2$ efflux. This respiratory "burst" occurred after the light-dependent increase in $O_2^{-\bullet}$ production and H_2O_2 accumulation in chloroplasts (Figure 6B, compare the red and pink curves, note that apparent "early" light response in data is an artifact from integrating data points over 30 s, all gas fluxes were integrated equally). Generation of $O_2^{-\bullet}$ and subsequent H_2O_2 formation also occurs in Complex-I of mitochondria, and can be specifically inhibited by rotenone, without affecting the TCA cycle or oxidative phosphorylation. To further probe the mitochondrial $^{12}CO_2$ efflux, we vacuum infiltrated leaves also with Cat and with rotenone. Neither compound affected the gas exchange trends of $^{12}CO_2$ efflux in comparison with untreated control discs (infiltrated with water) (Supplemental Figure S7, compare blue, pink and black curves). When leaves were infiltrated with MV + rotenone, samples exhibited a similar light-induced respiratory burst of $^{12}CO_2$ efflux as the standard MV infiltrated leaves (Figure 6C, compare the orange curve to the red curve in Supplemental Figure S7). Thus, the chloroplast originated H_2O_2 was an apparent cause for upregulation of mitochondrial $^{12}CO_2$ burst. However, leaves infiltrated with MV + Cat shared dynamics with DCMU and DBMIB infiltrated discs, showing no light-dependent burst of $^{12}CO_2$ efflux (Figure 6C, compare green and black curves with the green curve of Supplemental Figure S7). Therefore, the light-dependent $^{12}CO_2$ burst was only apparent following infiltration with MV and was not affected by rotenone but was blocked by Cat. This indicates that MV stops NADP reduction in chloroplasts and, due to an absence of NADPH, neither the formation nor the export of malate can take place from chloroplasts. We speculate this as a possible evidence for H_2O_2 signaling to mitochondria (Cui et al., 2019), relating to "malate cycling" (Zhao et al., 2020). It is conceivable that mitochondria are primed to process an influx of malate during a prolonged PSI acceptor limitation, providing a buffer to minimize ROS accumulation and damage at PSI (Noguchi and Yoshida, 2008). As no malate could form in leaves infiltrated with MV, due to an absence of NADP reduction, the primed mitochondria likely increased the rate of decarboxylation reactions due to an increased sink availability.

Discussion

ROS produced photosynthetically in chloroplast thylakoid membrane play a key role in photodamage, environmental sensing, and photosynthetic regulation. Within this paradigm, it is proposed that relatively stable ROS, such as H_2O_2, can be exported from the chloroplast to act directly as a signal in fine-tuning nuclear gene expression during plant

acclimation to changing environments (Exposito-Rodriguez et al., 2017; Gollan and Aro, 2020), or as a trigger for cellular processes such as stomatal closure (Wang et al., 2016; Iwai et al., 2019). Models of ROS signaling require that the sources of, and responses to (signaling pathway) specific ROS are well understood. While chloroplast H_2O_2 signaling pathways are slowly being defined (Rossel et al., 2007; Bechtold et al. 2008; Dietz et al., 2016; Crisp et al., 2017; Gollan and Aro, 2020), the endogenous sources of specific ROS in the thylakoid membrane and the environmental conditions that lead to their formation are still subject to debate. For example, the current literature supports the generation of a stable H_2O_2 pool, capable of export from the chloroplast, in multiple sites of PETC including the reduction of O_2 at PSII (Tiwari and Pospisil, 2009; Khorobrykh, 2019), the PQ pool (Khorobrykh and Ivanov, 2002; Mubarakshina and Ivanov, 2010; Khorobrykh et al., 2015), PTOX (Heyno et al., 2009), Cyt-b_6f complex (Baniulis et al., 2013), and PSI (Mehler, 1951; Kozuleva et al., 2020). This broad range of candidates complicates models of ROS signaling, resulting in debates like those between Wang et al. (2016) and Iwai et al. (2019). While both agree that stomatal closure is triggered by chloroplast-derived H_2O_2, the former argues in favor of reduced PQ as the source H_2O_2 and the latter concludes that it must be sourced from PSI. These discrepancies, together with our recent finding that the inhibitor DNP-INT, used historically in this field, fails to completely block re-reduction of $P700^+$ (Fitzpatrick et al., 2020) prompted us to re-evaluate the ROS formation by specific PETC components of the thylakoid membrane. As the application of DNP-INT in previous studies (Khorobrykh and Ivanov, 2002; Borisova-Mubarakshina et al., 2018) likely failed to fully inhibit the PSI Mehler reaction, artifacts may have been reported which could complicate the models of ROS signaling. By thoroughly testing the efficacy of all chosen inhibitors with P700 spectroscopy, and directly quantifying the simultaneous O_2 production and consumption reactions with MIMS, we have taken here an approach to measuring site-specific ROS formation within the PETC, and particularly the accumulation of H_2O_2, which minimizes the number of assumptions to be made during analysis.

H_2O_2 accumulation via O_2 photoreduction in isolated thylakoids occurs exclusively at PSI

Measuring the stoichiometry of O_2 produced and consumed by isolated thylakoids during illumination enabled the calculation of an O_2 flux ratio, which was anticipated to reach 1:2 when H_2O_2 accumulated as described previously by Allen (1977) and Asada (1999, 2006) (Figure 1). As expected, we observed a 1:2 O_2 flux ratio in untreated control and MV-treated thylakoid samples (Figures 3H and 4E). Further addition of Cat to these thylakoid samples pushed the ratio back to 1:1 (Figure 3, B and D), confirming that accumulation of H_2O_2 was responsible for the observed 1:2 O_2 flux ratio. This result fully supports the known fact that the PSI Mehler reaction generates H_2O_2 (Mehler, 1951). In stark contrast to O_2 flux results with control- and MV-treated thylakoids, the isolated thylakoids incubated with $HgCl_2$ and DBMIB, which we demonstrated with concomitant measurements of P700 redox kinetics to completely block all PSI function (Figure 2, A and B), exhibited 1:1 O_2 flux ratios. These stoichiometric O_2 production and consumption experiments undoubtedly demonstrate that efficient inter-chain PETC inhibitors completely block the accumulation of H_2O_2 and, conversely, a stable pool of H_2O_2 can be acquired in isolated thylakoids only via the activity of PSI.

Separating the formation of H_2O_2 from its accumulation within the thylakoid membrane

Stable accumulation of H_2O_2 produced a 1:2 O_2 flux ratio in our experiments, being consistent to support the function of a putative direct H_2O_2 retrograde signal. In contrast, the 1:1 O_2 flux ratio that implies no stable accumulation of H_2O_2 for export, questions the involvement of thylakoid components upstream of PSI in the H_2O_2 related long distance regulatory processes. However, a substantial body of previous research suggests that H_2O_2 can form upstream of PSI (the PQ pool [Khorobrykh and Ivanov, 2002; Mubarakshina and Ivanov, 2010; Khorobrykh et al., 2015], PTOX [Heyno et al., 2009], and Cyt-b_6f complex [Baniulis et al., 2013]). While our data seem to contradict these works, we postulate that the discrepancies merely highlight a difference in our approach, which relies on the strength of the MIMS data in separating H_2O_2 *formation* from H_2O_2 *accumulation*. Recall that illumination of control and MV treated thylakoid samples generated substantial quantities of H_2O_2 (Figure 3, A and C), yet a 1:1 O_2 flux ratio was observed in the presence of Cat (Figure 3, B and D). In the same manner, it is plausible that H_2O_2 may form within the thylakoid membrane upstream of PSI as previously suggested (Khorobrykh and Ivanov, 2002; Heyno et al., 2009; Mubarakshina and Ivanov, 2010; Baniulis et al., 2013; Khorobrykh et al., 2015). Nevertheless, the MIMS data unequivocally show that such H_2O_2 is not stable and must be rapidly broken down, analogous to the Cat-treated control samples. Importantly, PSII oxygen evolution was active in the presence of DBMIB and $HgCl_2$ (Figure 3, B and D), making it plausible that $O_2^{-\bullet}$ was formed and, therefore, also H_2O_2 was apparently being transiently produced in the absence of PSI. It is conceivable that such unstable H_2O_2 may be positively detected by sensitive dyes (Cathcart et al., 1983), spin-traps, specific sensor proteins (Villamena and Zweier, 2004), or other sensitive methods of H_2O_2 detection. For this reason, the capacity of the MIMS method to discriminate between H_2O_2 that accumulated, versus H_2O_2 that briefly formed, is an important distinction from the perspective of the putative H_2O_2 retrograde signal.

Pathway(s) of O_2 photoreduction within the thylakoid membrane

MIMS measurements of thylakoid samples incubated with $HgCl_2$ (Figures 3G and 4H) and both thylakoid and leaf

samples incubated with DBMIB (Figures 3F, 4G, and 6D) maintained steady-state O_2 production during illumination. This PSII activity was associated with commensurate O_2 consumption resulting in a 1:1 O_2 flux ratio. Both DBMIB- and $HgCl_2$-treated thylakoid samples exhibited similar O_2 flux rates at GL which did not increase during HL illumination in the DBMIB-treated samples, a dynamic also observed in DBMIB infiltrated leaf discs (Figure 6D; Supplemental Table S1). Conversely, the O_2 flux rate doubled in response to HL in the $HgCl_2$ thylakoid samples (Supplemental Figure S1, direct comparison of thylakoid samples). As the PSII contribution to $O_2^{-\bullet}$ formation is relatively low (Khorobrykh, 2019), the DBMIB pathway (excluding Cyt-b_6f) tested the maximum rate of O_2 reduction resulting from direct interaction between reduced Q_A, Q_B or the PQ pool, and O_2, potentially via the theorized PQH_2/PQH^- $O_2^{-\bullet}$ formation and quenching mechanism (Khorobrykh and Tyystjärvi, 2018), and/or directly via PTOX (Cournac et al., 2000). That the rate was saturated at a low irradiance was consistent with in vitro characterizations of the PTOX pathway (Nawrocki et al., 2015). In comparison, the reduction of PQ pool and Cyt-b_6f in $HgCl_2$-treated thylakoids corresponded to an increased rate of both O_2 production and consumption at HL, which supports the widely held hypothesis that Cyt-b_6f can generate $O_2^{-\bullet}$ as demonstrated by Baniulis et al. (2013) (as $HgCl_2$ was toxic for leaf discs, a direct comparison between in vitro and in vivo $HgCl_2$ samples was impossible). We unexpectedly found that application of the specific PTOX inhibitors *n*-propyl- and octyl-gallate increased the rates of both O_2 production and consumption (Supplemental Figure S4), confounding our attempt to examine the specific contribution of PTOX to the rate of O_2 reduction. The absence of an EPR spin-trap signal in $HgCl_2$-treated thylakoids supports a route of catalyzed O_2 reduction within the thylakoid membrane, possibly at PTOX (Figure 5B, green curve). These results suggest that (1) thylakoid membranes apparently support at least two separate routes of O_2 reduction upstream of PSI, (2) both routes of O_2 reduction exhibit a lower absolute capacity than the PSI Mehler reaction, and (3) none of the O_2 reduction pathways upstream of PSI produce a stable pool of H_2O_2 that could be exported as a retrograde signal.

A simpler model for H_2O_2 signaling

Our conclusions broadly support what is already described regarding the *formation* of ROS by photosynthetic processes in the chloroplast (Kozuleva et al., 2020), including our observation of multiple distinct pathways for ROS formation associated with the thylakoid membrane. We have not ruled out that $O_2^{-\bullet}$ and possibly H_2O_2 form upstream of PSI and can be detected by rapidly reacting dyes (Cathcart et al., 1983), spin-traps, or specific sensor proteins (Villamena and Zweier, 2004). Despite this, our results dismiss the possibility that any stable pool of H_2O_2 can *accumulate* upstream of PSI. This finding has important consequences for models of chloroplast H_2O_2 retrograde signaling, as it implies that any H_2O_2 exported from the chloroplast was formed at PSI. In the absence of added Fd, isolated thylakoid samples do not exhibit strong rates of O_2 reduction (Furbank and Badger, 1983). This implicates the acceptor side of PSI in $O_2^{-\bullet}$ formation. In addition, activity of O_2 reduction was efficiently quenched by the addition of $NADP^+$ (Furbank and Badger, 1983), suggesting that the acceptor side capacity of PSI regulates the rate of $O_2^{-\bullet}$ formation. As no other potential source of H_2O_2 formation could generate a stable H_2O_2 pool within the thylakoid membrane during our experiments, the data suggest that only the PSI acceptor side contributes to H_2O_2 involved in direct H_2O_2 retrograde signaling (Exposito-Rodriguez et al., 2017; Gollan and Aro, 2020). Therefore, the export of H_2O_2 from the chloroplast specifically communicates PSI acceptor limitation to the broader cell.

Based on the available data, we propose that H_2O_2 sufficiently accumulates for export from chloroplasts only under conditions where PSI acceptors are fully reduced, and the antioxidant pathways of the WWC have become overwhelmed. This is in line with the absence of Cat (which does not require reductant to function or exhibits H_2O_2 sensitivity; Mhamdi et al., 2010) from chloroplasts, which instead rely on pathways of H_2O_2 detoxification that are sensitive to excess H_2O_2 accumulation (Kitajima et al., 2010). In this model, the peroxiredoxin, ascorbate, and ascorbate peroxidase enzymes of the Mehler WWC act as a buffer, decreasing the sensitivity of any chloroplast-derived H_2O_2 signal to short term and transitory stress events. Therefore, any H_2O_2 retrograde signal, which is the quickest to trigger a regulatory response during HL stress (Gollan and Aro, 2020), only forms once environmental conditions potentially leading to PSI damage start to dominate (Tiwari et al., 2016). Such a mechanism avoids nuclear responses during transient stresses, such as sun flecks or patchy cloud cover. This avoids potentially premature downregulation of key photosynthetic processes such as light-harvesting (Borisova-Mubarakshina et al., 2015) during otherwise low-light conditions. While short-term stress events can be mitigated via the enzymes of the WWC and other regulatory processes such as nonphotochemical quenching and photosynthetic control at Cyt-b_6f (Shimakawa and Miyake, 2018), longer term environmental shifts that lead to chronic overreduction of the PSI acceptor pool will result in the deactivation of the WWC's antioxidant enzymes, followed by accumulation and eventual export of H_2O_2. In this model, the PSI acceptor side-specific H_2O_2 retrograde signal is a mechanism to convey information from chloroplasts to the nucleus when dominant environmental conditions change and the PSI acceptor side faces chronic limitation. This provides the nucleus with a mechanism to efficiently respond for acclimation to a new environment, while avoiding nuclear responses to short-term perturbations such as sun flecks.

Possible evidence of direct H_2O_2-triggered cooperation between chloroplast and mitochondria

In order to estimate the O_2 flux ratio associated specifically with the Mehler reaction of leaf discs, we artificially enriched

the leaf disc sample atmosphere to 2% with $^{13}CO_2$. This enabled us to discriminate between photosynthetic assimilation of $^{13}CO_2$ and the efflux of respiratory $^{12}CO_2$ (Figure 6). With this method, we observed that leaf discs infiltrated with MV exhibited a sharp increase in $^{12}CO_2$ efflux from mitochondrial respiration during illumination. The light dependant burst of $^{12}CO_2$ efflux was absent in leaves infiltrated with DCMU or DBMIB, excluding oxidation of the PSI acceptor side as a cause. The $^{12}CO_2$ burst was maintained in leaves infiltrated with MV + Rotenone, yet inhibited when leaves were infiltrated with both MV + Cat. These results suggest that H_2O_2 formed by MV at the acceptor side of PSI may have triggered an increase in mitochondrial respiration. This fits with a growing body of evidence that mitochondria and chloroplasts interact to optimize the photosynthetic performance. From an efficiency perspective, the organelles co-locate to improve C_3 photosynthesis by maximizing the assimilation of respired CO_2 (Busch et al., 2013). From a regulatory perspective, it has long been known that mitochondria can accept excess electrons from the chloroplast thylakoid membrane in leaves (Noguchi and Yoshida, 2008) and it was recently confirmed that mitochondrial AOX expression reduces ROS damage, and was necessary for HL acclimation in green algae (Kaye et al., 2019). In chloroplasts, under efficient NADPH generation in reducing conditions like HL, oxaloacetate is reduced to malate by plastidial NADPH-dependent malate dehydrogenase. Malate can be easily transported through subcellular membranes to cytosol and other organelles serving as a substrate for ATP and NADH production (Selinski and Scheibe, 2019), thus functioning as a powerful transporter of reducing equivalents across cellular compartments and controlling redox balance and metabolism between mitochondria and chloroplasts. The term "malate circulation" has been proposed (Zhao et al., 2020) to describe the various regulatory functions spanning both organelles, potentially including programmed cell death, that relate to the "malate valve" (Selinski and Scheibe, 2019).

To explain our observation that MV infiltration increased the CO_2 efflux measured from leaf discs during illumination in a Cat sensitive manner, we propose that H_2O_2 produced by MV was exported from the chloroplast, which then triggered upregulation or "priming" of an oxidative pathway in surrounding mitochondria, potentially AOX (based on work with *Chlamydomonas* [Kaye et al., 2019]). Therefore, the mitochondria were primed by artificially produced H_2O_2; the upregulated pathway increased the oxidative sink capacity within the mitochondria. To satisfy this increased sink, the rate of decarboxylation reactions may have been upregulated, an effect already observed in mitochondria in the absence of photosynthesis (Scarpeci and Valle, 2008).

It is conceivable that the pre-incubation with MV contributed to priming this response, hence its rapid activation during illumination, although the speed of the response may be evidence that this is a critical pathway to facilitate protection of PSI during acute acceptor limitation. It precedes down-regulation of photosynthetic processes triggered by H_2O_2 retrograde signaling, which take at least half an hour (Gollan and Aro, 2020), during which time the interaction may function to provide the PSI acceptor side with either $NADP^+$ via the malate valve (Noguchi and Yoshida, 2008), or CO_2 via the upregulated carboxylation reactions observed during our measurements. The latter response could be of great significance if the stomata also close due to a H_2O_2 trigger (Iwai et al., 2019). This explanation fits our proposed model of PSI-specific H_2O_2 signaling. It suggests that H_2O_2 export from the chloroplast simultaneously signals down regulation of photosynthetic processes during prolonged acceptor limitation and upregulation of a pathway to temporarily increase the PSI acceptor capacity via the malate valve and potentially directly via the increased availability of respired CO_2.

Concluding remarks

We have demonstrated that H_2O_2 can accumulate in the thylakoid membrane only via the PSI Mehler reaction. Accumulation and a long lifetime of H_2O_2 make it possible for H_2O_2 to migrate from one cellular location to another. This explicitly excludes the involvement of other PETC components in chloroplastic H_2O_2 signaling pathways, with substantial implications for models of H_2O_2 involvement in processes like stomatal regulation or retrograde signaling. We have confirmed the function of separate O_2 consumption pathways within the thylakoid membrane, involving the PQ pool and Cyt-b_6f, yet neither of them demonstrated the capacity to accumulate H_2O_2. We propose a model for chloroplastic H_2O_2 signaling based on the PSI acceptor side capacity. This enables efficient nuclear regulation in response to chronic environmental changes, while avoiding unnecessary responses to short-term stress caused by conditions such as sun-flecks or patchy cloud cover. Finally, we have discovered potential evidence for H_2O_2-triggered cooperation between the chloroplast and mitochondria. We suggest that this may alleviate PSI acceptor side stress when the antioxidant systems of the WWC are overwhelmed and PSI is more susceptible to damage.

Materials and methods

Plant material and thylakoid isolation

The Arabidopsis (*A. thaliana*) plants were grown at atmospheric CO_2 under dark/light cycle of 16/8 h at 120 µmol photons m^{-2} s^{-1}. Thylakoids were isolated from 6 weeks old plants using standard method as described earlier (Tiwari et al., 2016). All measurements were performed with freshly isolated thylakoids in measurement buffer containing: 330 mM sorbitol, 5 mM $MgCl_2$, 10 mM NaCl, 5 mM NH_4Cl, 50 mM Hepes pH 7.6, unless stated otherwise. Measurements on intact leaf or leaf discs on Dual Pam and MIMS were performed using the same plants. For infiltration of electron transfer inhibitors/modulators in leaves, detached leaves were floated at 25°C in darkness for 1 h in either H_2O

(control) or H_2O + 10 μM DBMIB or H_2O + 10 μM DNP-INT, or H_2O + 10 μM MV.

P700 redox kinetics measurements

Detached leaves and isolated thylakoids were used for P700 redox kinetics measurements using Dual-Pam-100 (Heinz Walz GmbH, Effeltrich, Germany). The P700 was oxidized under continuous FR light. The partial and complete re-reduction of P700 by electrons flow from PSII was achieved by shooting two short pulses of SPs that is, ST 50 μs and MT 50 ms, over the FR light oxidized P700 (Tiwari et al., 2016).

Superoxide measurement

Spin trapping for $O_2^{-\bullet}$ was performed in isolated thylakoids using Miniscope (MS5000) EPR-spectrometer equipped with variable temperature controller (TC-HO4) and Hamamatsu light source (LC8). The isolated thylakoids equivalent to 150 μg mL^{-1} Chl were illuminated under actinic light (150 μmol photons m^{-2} s^{-1}) for 180 s in the presence of DIPPMPO spin trap (50 mM) in 50 mM Hepes-NaOH (pH 7.5) with 50 μM desferal. Subsequently, the samples were centrifuged at 6,500 × g for 5 min and supernatant was used for EPR measurements. The electron transport inhibitors DCMU (10 μM), DBMIB (10 μM), DNP-INT (10 μM), $HgCl_2$ (2 mg mL^{-1}), and MV (10 μM) were added in reaction medium when indicated prior to the measurements. The measurements were conducted at frequency 9.41 GHz, center field 3,363 G, field sweep 150 G, microwave power 3 mW, and modulation frequency of 100 kHz with modulation width of 2 G. A minimum three to five independently isolated thylakoid samples were used for the final spectra and five accumulations were recorded from each sample.

Gas exchange measurements in liquid samples

The MIMS liquid cuvette consisted of an in-house modified Hansatech O_2 electrode body, with the silver/platinum electrode replaced by a stainless-steel assembly supporting a Teflon membrane (Hansatech, King's Lynn, UK) attached directly to the High Vacuum inlet of a Thermo Sentinel-PRO magnetic sector mass spectrometer (Thermo-Fisher, Waltham, MA, USA), collecting masses 32 and 36 with a total cycle time of ∼4.5 s. Freshly isolated thylakoid was stored on ice in darkness. For each run sufficient measurement buffer (containing: 330 mM sorbitol, 5 mM $MgCl_2$, 10 mM NaCl, 5 mM NH_4Cl, and 50 mM Hepes pH 7.6) was loaded into the cuvette with the addition, via syringe (∼50 μg mL^{-1} chlorophyll) to a final volume of 1,000 μL. In darkness the sample was purged with N_2 to minimize background $^{16}O_2$ before a bubble of $^{18}O_2$ (99% Cambridge Isotope Laboratories Inc, UK) was loaded into the stirring liquid, bringing the concentration of the heavier isotope up to approximately 150 nmol mL^{-1}. The bubble was removed and inhibitors were injected at this moment (10 μM DCMU, 10 μM MV, 10 μM DBMIB, and 10 μM DNP-INT). Samples were illuminated via halogen lamp (Dolan Jenner, USA) at low light (120 μmol photons m^{-2} s^{-1}) or HL (900 μmol photons m^{-2} s^{-1}). At the end of each run, the Chl concentration of each sample was determined in triplicate using the Porra Method (Porra et al., 1989) in 90% (v/v) MeOH to ensure accurate normalization of rates between samples. The cuvette was washed thoroughly with multiple rinses of 70% (v/v) ethanol followed by MQ H_2O when changing between inhibitors to avoid cross contamination. All data were analyzed and fluxes calculated with equations described in Beckmann et al. (2009), which includes offsets for the changing relative concentrations of $^{16}O_2$ and $^{18}O_2$, while any background O_2 consumption produced by thylakoid samples was normalized to zero in darkness as per (Furbank and Badger, 1983).

Gas exchange measurements in leaf discs

Gas fluxes from intact leaf discs in an atmosphere enriched in two stable isotopes, $^{18}O_2$ and $^{13}CO_2$, were performed using MIMS in an in-house built 1,000 μL gas-phase cuvette connected to the same mass spectrometer, collecting masses 32, 36, 44, and 45 with a cycle time of ∼6 s. A 14 mm diameter leaf discs cut from fully developed wild type Arabidopsis plants floated in darkness for 4 h in a dish of H_2O (control), H_2O + MV (10 μM), H_2O + DBMIB (20 μM), and H_2O + DCMU (10 μM) at ∼20°C. For leaf disc samples infiltrated with Cat, SHAM, and rotenone, discs were vacuum infiltrated before being allowed to dry on damp tissue in darkness for ∼1 h (until discs were no longer transparent). For all samples, in minimal light, a 12.5-mm disc was cut from the incubated 14 mm discs and loaded into the pre-calibrated cuvette at 25°C. In darkness, the samples were purged with atmospheric air scrubbed of endogenous $^{12}CO_2$ (Soda Lime, Li-Cor, USA), the cuvette was then enriched to approximately 2% $^{13}CO_2$ and 3% $^{18}O_2$ by volume, with the remainder of the atmosphere comprising approximately standard atmospheric concentrations. The very low $^{12}CO_2$ partial pressure in the beginning of measurements minimized membrane consumption of this isotope to almost zero, enabling the rate of its production in darkness (mitochondrial respiration) to be used as a basis for setting the background consumption rate of $^{18}O_2$ (mitochondrial respiration in dark, plus Mehler reaction during illumination). Rates of $^{16}O_2$ (PSII water splitting) and $^{13}CO_2$ (CO_2 fixation by Rubisco) were both set to zero in darkness. The enriched CO_2 atmosphere avoided photorespiration, while an approximately atmospheric level of O_2 was maintained to maximize the probability of observing Mehler-associated O_2 reduction, with the same offsets for steady dilution of the stable isotopes used in calculations of steady-state fluxes as described for liquid phase measurements. Following initiation of data acquisition, samples experienced 3 min of darkness, 5 min of GL (120 μmol photons m^{-2} s^{-1}), 5 min of HL (900 μmol(photons) m^{-2} s^{-1}), and then 4 min of darkness. Rates were calculated according to equations described in Beckmann et al. (2009).

Supplemental data

The following materials are available in the online version of this article.

Supplemental Figure S1. Direct comparison of O_2 evolution rates by thylakoid membranes incubated with DBMIB (10 μM) and $HgCl_2$ (2 mg mL^{-1}) at 120 and 900 μmol photons m^{-2} s^{-1}.

Supplemental Figure S2. Interpreting time-resolved gas fluxes, examining the post illumination $^{18}O_2$ burst as further evidence of H_2O_2 accumulation.

Supplemental Figure S3. Plotting integrated peak area and steady-state O_2 evolution rate as functions of DBMIB concentration.

Supplemental Figure S4. Investigation into the effects of *n*-propyl gallate and octyl gallate applied at 0.5 mM to isolated thylakoid membranes.

Supplemental Figure S5. Impact of HL on isolated thylakoid samples treated with Cat was consistent for all measured samples.

Supplemental Figure S6. Gas fluxes measured in a blank cuvette.

Supplemental Figure S7. Comparison of mitochondrial $^{12}CO_2$ efflux from vacuum-infiltrated leaf discs.

Supplemental Table S1. Average steady-state approximation of rates of gas exchange in μmol m^{-2} s^{-1} in leaf discs.

Funding

Research was funded by the Jane and Aatos Erkko Foundation and the Center of Excellence program of the Academy of Finland (project no 307335).

Conflict of interest statement. Authors declare no conflict of interest.

References

Allen J (1977) Oxygen—a physiological electron acceptor in photosynthesis? Curr Adv Plant Sci **9:** 459–469

Asada K (2006) Production and scavenging of reactive oxygen species in chloroplasts and their functions. Plant Physiol **141:** 391–396

Asada K (1999) THE WATER–WATER CYCLE IN CHLOROPLASTS: Scavenging of active oxygens and dissipation of excess photons. Annu Rev Plant Physiol Plant Mol Biol **50:** 601–639

Baniulis D, Hasan SS, Stofleth JT, Cramer WA (2013) Mechanism of enhanced superoxide production in the cytochrome b(6)f complex of oxygenic photosynthesis. Biochemistry **52:** 8975–8983

Bauer R, Wijnands MJG (1974) The inhibition of photosynthetic electron transport by DBMIB and its restoration by *p*-phenylenediamines; studied by means of prompt and delayed chlorophyll fluorescence of green algae. Z Naturforsch C J Biosci **29:** 725–732

Bechtold U, Richard O, Zamboni A, Gapper C, Geisler M, Pogson B, Karpinski S, Mullineaux PM (2008) Impact of chloroplastic- and extracellular-sourced ROS on high light-responsive gene expression in Arabidopsis. J Exp Bot **59:** 121–133

Beckmann K, Messinger J, Badger MR, Wydrzynski T, Hillier W (2009) On-line mass spectrometry: Membrane inlet sampling. Photosynth Res **102:** 511–522

Borisova-Mubarakshina M, Ivanov BN, Vetoshkina DV, Lubimov VY, Fedorchuk TP, Naydov IA, Kozuleva MA, Rudenko NN, Dall'Osto L, Cazzaniga S, et al. (2015) Long-term acclimatory response to excess excitation energy: Evidence for a role of hydrogen peroxide in the regulation of photosystem II antenna size. J Exp Bot **66:** 7151–7164

Borisova-Mubarakshina MM, Naydov IA, Ivanov BN (2018) Oxidation of the plastoquinone pool in chloroplast thylakoid membranes by superoxide anion radicals. FEBS Lett **592:** 3221–3228

Busch FA, Sage TL, Cousins AB, Sage RF (2013) C3 plants enhance rates of photosynthesis by reassimilating photorespired and respired CO_2. Plant Cell Environ **36:** 200–212

Carpentier R (2001) The negative action of toxic divalent cations on the photosynthetic apparatus. *In* M Passarakli, ed, Handbook of Plant and Crop Stress, Marcel Dekker, New York, NY, pp 763–772

Cathcart R, Schwiers E, Ames BN (1983) Detection of picomole levels of hydroperoxides using a fluorescent dichlorofluorescein assay. Anal Biochem **134:** 111–116

Chalier F, Tordo P (2002) 5-Diisopropoxyphosphoryl-5-methyl-1-pyrroline *N*-oxide, DIPPMPO, a crystalline analog of the nitrone DEPMPO: Synthesis and spin trapping properties. J Chem Soc Perkin Trans **2:** 2110–2117

Cournac L, Josse EM, Joët T, Rumeau D, Redding K, Kuntz M, Peltier G (2000) Flexibility in photosynthetic electron transport: A newly identified chloroplast oxidase involved in chlororespiration. Philos Trans R Soc Lond B Biol Sci **355:** 1447–1454

Crisp PA, Ganguly DR, Smith AB, Murray KD, Estavillo GM, Searle I, Ford E, Bogdanović O, Lister R, Borevitz JO, et al. (2017) Rapid recovery gene downregulation during excess-light stress and recovery in Arabidopsis. Plant Cell **29:** 1836–1863

Cui F, Brosché M, Shapiguzov A, He X, Vainonen JP, Leppälä J, Trotta A, Kangasjärvi S, Salojärvi J, Kangasjärvi J, et al. (2019) Interaction of methyl viologen-induced chloroplast and mitochondrial signalling in Arabidopsis. Free Radic Biol Med **134:** 555–566

Dietz K, Mittler R, Noctor G (2016) Recent progress in understanding the role of reactive oxygen species in plant cell signaling. Plant Physiol **171:** 1535–1539

Durrant JR, Giorgi LB, Barber J, Klug DR, Porter G (1990) Characterisation of triplet states in isolated Photosystem II reaction centres: Oxygen quenching as a mechanism for photodamage. Biochim Biophys Acta **1017:** 167–175

Exposito-Rodriguez M, Laissue PP, Yvon-Durocher G, Smirnoff N, Mullineaux PM (2017) Photosynthesis-dependent H(2)O(2) transfer from chloroplasts to nuclei provides a high-light signalling mechanism. Nat Commun **8:** 49–49

Farquhar GD, Busch FA (2017) Changes in the chloroplastic CO2 concentration explain much of the observed Kok effect: a model. New Phytol **214:** 570–584

Fichman Y, Miller G, Mittler R (2019) Whole-plant live imaging of reactive oxygen species. Mol Plant **12:** 1203–1210

Fitzpatrick D, Aro E, Tiwari A (2020) A commonly used photosynthetic inhibitor fails to block electron flow to photosystem I in intact systems. Front Plant Sci **11:** 382

Furbank RT, Badger MR (1983) Oxygen exchange associated with electron transport and photophosphorylation in spinach thylakoids. Biochim Biophys Acta **723:** 400–409

Gollan PJ, Aro EM (2020) Photosynthetic signalling during high light stress and recovery: Targets and dynamics. Philos Trans R Soc Lond B Biol Sci **375:** 20190406

Halliwell B, Gutteridge JM (1984) Oxygen toxicity, oxygen radicals, transition metals and disease. Biochem J **219:** 1–14

Heyno E, Gross CM, Laureau C, Culcasi M, Pietri S, Krieger-Liszkay A (2009) Plastid alternative oxidase (PTOX) promotes oxidative stress when overexpressed in tobacco. J Biol Chem **284:** 31174–31180

Ilík P, Pavlovič A, Kouřil R, Alboresi A, Morosinotto T, Allahverdiyeva Y, Aro EM, Yamamoto H, Shikanai T (2017) Alternative electron transport mediated by flavodiiron proteins is operational in organisms from cyanobacteria up to gymnosperms. New Phytol **214:** 967–972

Iwai S, Ogata S, Yamada N, Onjo M, Sonoike K, Shimazaki K (2019) Guard cell photosynthesis is crucial in abscisic acid-induced stomatal closure. Plant Direct **3:** e00137

Kaye Y, Huang W, Clowez S, Saroussi S, Idoine A, Sanz-Luque E, Grossman AR (2019) The mitochondrial alternative oxidase from *Chlamydomonas reinhardtii* enables survival in high light. J Biol Chem **294:** 1380–1395

Khorobrykh A (2019) Hydrogen peroxide and superoxide anion radical photoproduction in PSII preparations at various modifications of the water-oxidizing complex. Plants (Basel, Switzerland) **8:** 329

Khorobrykh SA, Ivanov BN (2002) Oxygen reduction in a plastoquinone pool of isolated pea thylakoids. Photosynth Res **71:** 209–219

Khorobrykh SA, Khorobrykh AA, Yanykin DV, Ivanov BN, Klimov VV, Mano J (2011) Photoproduction of catalase-insensitive peroxides on the donor side of manganese-depleted photosystem II: evidence with a specific fluorescent probe. Biochemistry **50:** 10658–10665

Khorobrykh SA, Karonen M, Tyystjärvi E (2015) Experimental evidence suggesting that H_2O_2 is produced within the thylakoid membrane in a reaction between plastoquinol and singlet oxygen. FEBS Lett **589:** 779–786

Khorobrykh S, Tyystjärvi E (2018) Plastoquinol generates and scavenges reactive oxygen species in organic solvent: potential relevance for thylakoids. Biochim Biophys Acta **1859:** 1119–1131

Kimimura M, Katoh S (1972) Studies on electron transport associated with Photosystem I. I. Functional site of plastocyanin: Inhibitory effects of $HgCl_2$ on electron transport and plastocyanin in chloroplasts. Biochim Biophys Acta **283:** 279–292

Kitajima S, Nii H, Kitamura M (2010) Recombinant stromal APX defective in the unique loop region showed improved tolerance to hydrogen peroxide. Biosci Biotechnol Biochem **74:** 1501–1503

Kozuleva MA, Ivanov BN, Vetoshkina DV, Borisova-Mubarakshina M (2020) Minimizing an electron flow to molecular oxygen in photosynthetic electron transfer chain: An evolutionary view. Front Plant Sci **11:** 211

Lozier RH, Butler WL (1972) The effects of dibromothymoquinone on fluorescence and electron transport of spinach chloroplasts. FEBS Lett **26:** 161–164

Malkin R (1981) Redox properties of the DBMIB—Rieske iron—sulfur complex in spinach chloroplast membranes. FEBS Lett **131:** 169–172

Mehler AH (1951) Studies on reactions of illuminated chloroplasts. I. Mechanism of the reduction of oxygen and other Hill reagents. Arch Biochem Biophys **33:** 65–77

Mhamdi A, Queval G, Chaouch S, Vanderauwera S, Van Breusegem F, Noctor G (2010) Catalase function in plants: a focus on Arabidopsis mutants as stress-mimic models. J Exp Bot **61:** 4197–4220

Mubarakshina Borisova MM, Kozuleva MA, Rudenko NN, Naydov IA, Klenina IB, Ivanov BN (2012) Photosynthetic electron flow to oxygen and diffusion of hydrogen peroxide through the chloroplast envelope via aquaporins. Biochim Biophys Acta **1817:** 1314–1321

Mubarakshina MM, Ivanov BN (2010) The production and scavenging of reactive oxygen species in the plastoquinone pool of chloroplast thylakoid membranes. Physiol Plant **140:** 103–110

Nawrocki WJ, Tourasse NJ, Taly A, Rappaport F, Wollman F (2015) The plastid terminal oxidase: its elusive function points to multiple contributions to plastid physiology. Annu Rev Plant Biol **66:** 49–74

Noguchi K, Yoshida K (2008) Interaction between photosynthesis and respiration in illuminated leaves. Mitochondrion **8:** 87–99

Porra RJ, Thompson WA, Kriedemann PE (1989) Determination of accurate extinction coefficients and simultaneous equations for assaying chlorophylls a and b extracted with four different solvents: Verification of the concentration of chlorophyll standards by atomic absorption spectroscopy. Biochim Biophys Acta **975:** 384–394

Rossel JB, Wilson PB, Hussain D, Woo NS, Gordon MJ, Mewett OP, Howell KA, Whelan J, Kazan K, Pogson BJ (2007) Systemic and intracellular responses to photooxidative stress in Arabidopsis. Plant Cell **19:** 4091–4110

Scarpeci TE, Valle EM (2008) Rearrangement of carbon metabolism in *Arabidopsis thaliana* subjected to oxidative stress condition: An emergency survival strategy. Plant Growth Regul **54:** 133–142

Selinski J, Scheibe R (2019) Malate valves: Old shuttles with new perspectives. Plant Biol J **21:** 21–30

Shapiguzov A, Nikkanen L, Fitzpatrick D, Vainonen JP, Gossens R, Alseekh S, Aarabi F, Tiwari A, Blokhina O, Panzarová K, et al. (2020) Dissecting the interaction of photosynthetic electron transfer with mitochondrial signalling and hypoxic response in the Arabidopsis rcd1 mutant. Philos Trans R Soc B Biol Sci **375:** 20190413

Shimakawa G, Miyake C (2018) Oxidation of P700 ensures robust photosynthesis. Front Plant Sci **9:** 1617

Telfer A, Oldham TC, Phillips D, Barber J (1999) Singlet oxygen formation detected by near-infrared emission from isolated photosystem II reaction centres: Direct correlation between P680 triplet decay and luminescence rise kinetics and its consequences for photoinhibition. J Photochem Photobiol B Biol **48:** 89–96

Tiwari A, Mamedov F, Grieco M, Suorsa M, Jajoo A, Styring S, Tikkanen M, Aro EM (2016) Photodamage of iron-sulphur clusters in photosystem I induces non-photochemical energy dissipation. Nat Plants **2:** 16035

Tiwari A, Pospisil P (2009) Superoxide oxidase and reductase activity of cytochrome b559 in photosystem II. Biochim Biophys Acta **1787:** 985–994

Villamena FA (2017) Chapter 5—EPR spin trapping. *In* FA Villamena, ed, Reactive Species Detection in Biology, Elsevier, Boston, MA, pp 163–202

Villamena FA, Zweier JL (2004) Detection of reactive oxygen and nitrogen species by EPR spin trapping. Antioxid Redox Signal **6:** 619–629

Wang W, He E, Chen J, Guo Y, Chen J, Liu X, Zheng H (2016) The reduced state of the plastoquinone pool is required for chloroplast-mediated stomatal closure in response to calcium stimulation. Plant J **86:** 132–144

Witt HT, Rumberg B, Junge W, Joliot P (1968) Electron Transfer, Field Changes, Proton Translocation and Phosphorylation in Photosynthesis. *In* B Hess, H Staudinger, eds, Biochemie des Sauerstoffs. Colloquium der Gesellschaft für Biologische Chemie, Vol 19. Springer, Berlin, Heidelberg

Zhao Y, Yu H, Zhou J, Smith SM, Li J (2020) Malate circulation: Linking chloroplast metabolism to mitochondrial ROS. Trends Plant Sci **25:** 446–454